Sulphate removal over barium-modified blast-furnace-slag geopolymer

Hanna Runtti[a], Tero Luukkonen[b], Mikko Niskanen[a], Sari Tuomikoski[a], Teija Kangas[a], Pekka Tynjälä[c], Emma-Tuulia Tolonen[a,b], Minna Sarkkinen[b], Kimmo Kemppainen[b], Jaakko Rämö[a] & Ulla Lassi[*a,c]

[a]*University of Oulu, Research Unit of Sustainable Chemistry, P.O. Box 3000, FI-90014 University of Oulu, Finland.*

[b]*Kajaani University of Applied Sciences, P.O. Box 52, FI-87101 Kajaani, Finland.*

[c]*University of Jyvaskylä, Kokkola University Consortium Chydenius, Unit of Applied Chemistry, Talonpojankatu 2B, FI-67100 Kokkola, Finland.*

*Corresponding author: E-mail: ulla.lassi@oulu.fi; tel. +358 40 029 4090

Abstract

Blast-furnace slag and metakaolin were geopolymerised, modified with barium or treated with a combination of these methods in order to obtain an efficient SO_4^{2-} sorbent for mine water treatment. Of prepared materials, barium-modified blast-furnace slag geopolymer (Ba-BFS-GP) exhibited the highest SO_4^{2-} maximum sorption capacity (up to 119 mg g^{-1}) and it compared also favourably to materials reported in the literature. Therefore, Ba-BFS-GP was selected for further studies and the factors affecting to the sorption efficiency were assessed. Several isotherms were applied to describe the experimental results of Ba-BFS-GP and the Sips model showed the best fit. Kinetic studies showed that the sorption process follows the pseudo-second-order kinetics. In the dynamic removal experiments with columns, total SO_4^{2-} removal was observed initially when treating mine effluent. The novel modification method of geopolymer material proved to be technically suitable in achieving extremely low concentrations of SO_4^{2-} (< 2 mg L^{-1}) in mine effluents.

Keywords: blast-furnace slag, metakaolin, geopolymer, adsorption, sulphate

1 Introduction

Sulphate (SO_4^{2-}) is a common anion in both natural water and industrial wastewater, such as acid mine drainage. Natural sources of SO_4^{2-} include the chemical weathering of sulphur-containing minerals and the oxidation of sulphides and sulphur [1–3]. SO_4^{2-} is non-toxic, and sulphur is a necessary mineral for several organisms. However, high concentrations of SO_4^{2-} in aqueous environments can cause the mineralisation of water, corrosion of reinforced steel, scaling of equipment and damage to mammals as well as endangering human health [1–4]. Under anaerobic conditions, SO_4^{2-} can be reduced to hydrogen sulphide (H_2S) by sulphate-reducing bacteria. H_2S is dangerous to environmental ecosystems due to its reactivity, toxicity and corrosivity [1, 4].

In Finland, the SO_4^{2-} limit in drinking water is set at 250 mg L^{-1}. However, the recommended maximum concentration is even lower (150 mg L^{-1}) to ensure that water pipes are not damaged [5]. Environmental agencies in many countries have set the maximum SO_4^{2-} concentration between 250 and 500 mg L^{-1} for both mine drainage and industrial effluents [2, 6]. When there is no established limit for SO_4^{2-}, limits for total dissolved solids (TDS) are usually defined, which means that SO_4^{2-} concentrations must comply with the TDS values [7]. In many countries, increasingly strict legislation has been introduced to control water pollution, so there is a need for effective SO_4^{2-} removal technologies.

The processes for SO_4^{2-} removal from wastewater include biological treatment with sulphate-reducing bacteria, membrane filtration (e.g. reverse osmosis), adsorption and/or ion exchange and chemical precipitation as gypsum, barium sulphate or ettringite. However, these methods suffer from limitations. For example, precipitation produces a large amount of potentially toxic sludge. Low concentrations (approx. 1200 to 2000 mg L^{-1}) cannot be removed by lime precipitation because of the solubility of the $CaSO_4$ that is produced [2, 8, 9]. In addition, biological treatment and ion exchange are costly [2, 3, 10, 11]. An adsorption system has the potential to be used in a so-called hybrid-system with precipitation, in which the remaining sulphate concentrations after the precipitation process could be removed via adsorption.

Adsorption may be preferred for SO_4^{2-} removal due to its simplicity, effectiveness and low cost [11, 12]. Suggested sorbents have included, for example, activated carbon [13], fly ash [14], limestone

[2, 15], minerals [3, 16–19], modified coir pith [6], modified rice straw [1], modified zeolites [20, 21], nano-alumina [22], soils [23–25] and waste materials [15].

Geopolymers are amorphous or partly crystalline inorganic polymers with a three-dimensional negatively charged framework structure, which is similar to zeolite [26–31]. They can be prepared at ambient or slightly elevated temperatures by the hydrothermal conversion of a solid aluminosilicate material, e.g. metakaolin [30, 32, 33], blast-furnace slag [34] or fly ash [29, 35–38] with an alkali hydroxide and/or silicate solution. In this study, blast-furnace slag (BFS) and metakaolin (MK) were used as a raw material for geopolymerisation. BFS is a residue product of smelting iron ore in a blast furnace and MK is a dehydroxylated form of the naturally occurring clay mineral kaolinite. BFS and MK are good raw material candidates for preparing geopolymers due to their abundance and easy availability [33, 34, 39, 40].

The series of geochemical reactions that comprise this process are not exactly known, but it has been suggested that they include mineral dissolution, aluminosilicate polycondensation and structural re-organisation [28, 29, 41–43]. Geopolymers possess permanent negative charges on Al on their structure that are balanced by exchangeable cations (e.g. Na^+, K^+, Li^+, Ba^{2+}) [43]. They have a high cation exchange capacity, which has been applied for the removal of metal(loid)s [32, 33, 35, 38, 44, 45], dyes [29] and ammonium [46], but there are no studies on SO_4^{2-} removal to our knowledge. Because geopolymers have a low affinity for anions, a chemical modification is needed to apply a sorbent for anionic SO_4^{2-} removal. In literature, it has been reported that the chemical modification with inorganic salts such as NaCl, $CaCl_2$, $BaCl_2$ or $FeCl_3$ improves properties of zeolites and increase its efficiency in water treatment [47–49]. In the present study, a similar approach was applied for geopolymer modification. In the case of anion removal, the modification has been reported to for example create an oxi-hydroxide adsorption layer on the surface and change the surface charge (from negative to positive) [49, 50]. These changes allow to form stable complexes with anions in solution. In the present study, the $BaCl_2$ modification was expected to impregnate Ba in the framework structure of geopolymers and subsequently enable the surface precipitation or complexation of sulphate.

In this study, the effects of geopolymerisation, barium modification and a combined treatment on metakaolin (MK) and blast-furnace slag (BFS) were studied in order to develop an efficient SO_4^{2-}

sorbent for mine effluent. Comparative experiments were first performed for synthetic water (model solution). The influence of initial pH, initial SO_4^{2-} concentration, sorbent dosage, contact time and temperature was studied. In addition, adsorption isotherms, kinetics and thermodynamic parameters were studied. Column studies were also performed for the most promising sorbent material: barium-modified BFS geopolymer (Ba-BFS-GP).

2 Experimental

2.1 Materials

BFS and MK were obtained from Finnish suppliers. Technical grade sodium hydroxide (VWR International) and sodium silicate (VWR International, SiO_2:Na_2O = 3.1–3.4) were used for the synthesis of geopolymers. NaCl and $BaCl_2$ were used in chemical modifications. A stock solution of SO_4^{2-} was prepared by dissolving Na_2SO_4 (VWR 99,9%) in ultrapure water and further diluted to concentrations required for the experiments. The pH of the solution was adjusted through the addition of HCl and/or NaOH (FF-Chemicals).

A mine effluent (settled drainage water treated with ferric sulphate) sample was obtained from an underground gold mine and it was characterized earlier [44].

2.2 Geopolymerisation

An alkaline solution containing 10 M NaOH and sodium silicate (SiO_2:Na_2O = 3.1–3.4) in a weight ratio of 1:1 was prepared 24 h before use. BFS or MK was mixed with the alkaline solution in a weight ratio of 3:2 or 1.3:1, respectively. The mixtures were mixed for 15 minutes, vibrated for 2 minutes and allowed to consolidate for 3 days at room temperature. The resulting solid material was crushed to a particle size of 63–125 µm or 0.5–1 mm for batch (equilibrium) and dynamic (non-equilibrium) experiments, respectively. Materials were washed with ultrapure water, dried at 105 °C and stored in a desiccator.

2.3 Chemical modification

The materials (5 g) were mixed with 1 M NaCl solution (50 mL) for 24 h, filtered, rinsed with deionised water and dried at 105 °C to ensure that all the ion exchange sites were in the Na form. Barium modification was conducted by mixing the material (5 g) in a 1 M $BaCl_2$ solution (100 mL) for 16 h, filtering, rinsing with deionised water and drying at 105 °C. The materials were ground and stored in a desiccator before use.

2.4 Characterisation of the sorbent

The specific surface area, total pore volume and average pore size were determined from nitrogen adsorption–desorption isotherms at the temperature of liquid nitrogen (-196 °C) using a Micromeritics ASAP 2020 instrument. The X-ray diffraction (XRD) patterns of materials were obtained using a PanAnalytical Xpert Pro diffractometer, and chemical compositions were determined using a PanAnalytical Minipal 4 X-ray fluorescence (XRF) spectrometer. Fourier Transform Infrared Spectroscopy (FTIR) spectra of the sorbent were collected using a Perkin Elmer Spectrum One spectrometer.

2.5 Batch sorption experiments

In the batch sorption experiments the system was allowed to reach the sorption equilibrium. The screening of potential sorbents Ba-modified metakaolin (Ba-MK), Ba-modified metakaolin geopolymer (Ba-MK-GP), Ba-modified blast-furnace slag (Ba-BFS) and Ba-modified blast-furnace-slag geopolymer (Ba-BFS-GP) was performed at different initial pH values in mine effluent. Initial pH was adjusted by using HCl and/or NaOH. Ba-BFS-GP was selected for further experiments: the effects of initial SO_4^{2-} concentration, sorbent dosage, temperature and contact time were studied. The studied parameters are shown in Table 1. Samples were filtrated through 0.45 µm filter paper (Sartorius Stedim Biotech) or separated using a centrifuge. SO_4^{2-} concentration was determined in the filtrate solution via ion

chromatography (Metrohm 761 Compact IC) or a flow injection analysis system (Foss-Tecator Fiastar 5000).

All experiments were run as duplicates, except experiments with mine effluent. The sorption experiments were performed in acid-washed vessels to minimise contamination.

Table 1. Parameters for testing the effects of initial pH, initial SO_4^{2-} concentration, sorbent dosage, contact time and temperature on SO_4^{2-} removal efficiency.

Parameter	Initial pH of solution	Initial SO_4^{2-} concentration [mg L^{-1}]	Sorbent dosage [g L^{-1}]	Contact time	Temperature [°C]	Sorbent	Water matrix
Effect of initial pH	4,6,8,10	850–870	5	24 h	22	Ba-MK, Ba-BFS, Ba-MK-GP, Ba-BFS-GP	Mine effluent*
Effect of initial SO_4^{2-} concentration	7–8	50–1000	5	24 h	22	Ba-BFS-GP	Synthetic
Effect of sorbent dosage	7–8	1200	0.5–15	3 h	10, 22, 40	Ba-BFS-GP	Synthetic
	7–8	865	0.5–25	24 h	22	Ba-BFS-GP	Mine effluent*
Effect of contact time	7–8	1100	5	1 min – 24 h	22	Ba-BFS-GP	Synthetic
	7–8	853	5	1 min – 24 h	22	Ba-BFS-GP	Mine effluent*

*There was a minor variation (850–870 mg L^{-1}) between the concentrations of different water samples.

2.6 Dynamic sorption experiments

In the dynamic experiments, the sorption was performed in the non-equilibrium state. The experiments were performed using a plastic column (diameter 44.0 mm, height 98.8 mm, volume 0.15 L), which was loaded with 30.45 g of Ba-BFS-GP with a particle size of 0.5–1 mm. The sorbent bed height was 2.0 cm with a bed volume of 30.41 cm^3. Mine effluent with 820 mg L^{-1} SO_4^{2-} was pumped through the column by a peristaltic pump. The flow of effluent was adjusted to 0.24 or 0.85 L h^{-1}, corresponding to 7.60 and 2.15 min empty bed contact time, respectively. Samples were taken from the outlet of the column at different time intervals.

2.7 Barium leaching test

To evaluate the stability of impregnated barium in Ba-BFS-GP, 0.125 g of material was added to 25 mL mine effluent and shaken 24 h. Barium leaching experiments were also performed with distilled water by weighing 0.005 or 0.125 g of Ba-BFS-GP to 10 mL or 25 mL of distilled water, respectively. Samples were filtered through 0.45 µm filter paper, and the barium concentration was analysed using inductively coupled plasma emission spectrometers (Thermo Electron IRIS Intrepid II XDL Duo or PerkinElmer Optima 5300 DV ICP-OES instrument) according to the SFS-EN ISO 11885 standard.

2.8 Adsorption isotherms

Bi-Langmuir [51], Sips [52], Redlich–Peterson (R–P) [53] and Toth [54] isotherms are presented in Equations 1–4, respectively. Isotherm parameters were obtained using nonlinear regression with the Microsoft Excel solver tool (GRG nonlinear).

$$q_e = \frac{q_{m_1} b_{L_1} C_e}{1+b_{L_1} C_e} + \frac{q_{m_2} b_{L_2} C_e}{1+b_{L_2} C_e}, \quad (1)$$

where q_{m1} and q_{m2} are the maximum adsorption capacities (mg g^{-1}) of two different adsorption sites. Similarly, b_{L1} and b_{L2} represent the energies (mg g^{-1}) of adsorption at these sites.

$$q_e = \frac{q_m (b_S C_e)^{n_s}}{1+(b_S C_e)^{n_s}}, \quad (2)$$

where b_S (L mg^{-1}) is a constant related to the adsorption energy and n_s is a dimensionless constant characterising the heterogeneity of the system.

$$q_e = \frac{K_R C_e}{1+a_R C_e^{\beta}}, , \quad (3)$$

where K_R (dm^3 g^{-1}) and a_R (dm^3 mg^{-1}) are R–P isotherm constants and β is an exponent, the value of which lies between 0 and 1.

$$q_e = \frac{q_{Th} K_{Th} C_e}{\left[1+(K_{Th} C_e)^{Th}\right]^{\frac{1}{Th}}}, \quad (4)$$

where q_m (mg g^{-1}) is the monolayer adsorptive uptake, K_{Th} (L mg^{-1}) is the Toth isotherm constant and *Th* is the dimensionless Toth isotherm exponent, which characterises the heterogeneity of the system.

The residual root mean square error (RMSE) and chi-square test (χ^2) were used to assess the error:

$$\mathrm{RMSE} = \sqrt{\frac{1}{n-p}\sum_{i=1}^{n}(q_{e(\exp)} - q_{e(calc)})^2}, \quad (5)$$

$$\chi^2 = \sum_{n=1}^{n} \frac{(q_{e(exp)} - q_{e(calc)})^2}{q_{e(calc)}}, \quad (6)$$

where n is the number of experimental data, p is the number of parameters whilst $q_{e(exp)}$ and $q_{e(calc)}$ are experimental and calculated values of adsorption capacity in equilibrium.

2.9 Kinetic modelling

The kinetics of the adsorption processes were studied using the pseudo-first-order [55], the pseudo-second-order [56] and the Elovich [57] kinetic models:

$$log(q_e - q_t) = log q_e - \frac{k_f}{2.303} t, \quad (7)$$

$$\frac{t}{q_t} = \frac{1}{k_s q_e^2} + \frac{1}{q_e} t, \quad (8)$$

$$q = \frac{1}{\beta}\ln\left(\upsilon_0\beta + \frac{1}{\beta}lnt\right), \quad (9$$

where q_e and q_t are the amounts of SO_4^{2-} sorbed (mg g^{-1}) at equilibrium and at time t (min), respectively. k_f (min^{-1}), k_s (g mg^{-1} min^{-1}) and υ_0 (mg g^{-1} min^{-1}) are the pseudo-first-order, pseudo-second-order and Elovich rate constants, respectively. The Elovich parameter β (g mg^{-1}) is related to the extent of surface coverage and activation energy for chemisorption.

The diffusion mechanism was analysed using the intraparticle diffusion model [58]:

$$q_t = k_{id}t^{1/2} + C, \quad (10)$$

where k_{id} (mg $g^{-1}min^{-1/2}$) is the intraparticle diffusion on the rate determining step and C is the intercept related to the thickness of the boundary layer.

2.10 Sorption thermodynamics

The change in free energy (ΔG), enthalphy (ΔH) and entropy (ΔS) were determined to describe the sorption of SO_4^{2-}:

$$\Delta G = -RTln(K_c), \quad (11)$$

$$K_c = \frac{q}{C_e}, \quad (12)$$

$$\ln K = \frac{\Delta S}{R} - \frac{\Delta H}{RT}, \quad (13)$$

where, R is the universal gas constant (8.314 J mol^{-1} K^{-1}), T is the temperature (K), and K_c is the equilibrium constant.

3 Results and discussion

3.1 Sorbent characterisation

Specific surface area, average pore size and volumes (Table 2) of MK increase as a result of geopolymerisation. However, with BFS, the surface area and pore volumes increase whereas pore size decreases during geopolymerisation. Barium modification has no significant effect on surface area, pore sizes and volumes of geopolymerised BFS.

Table 2. Specific surface areas, pore sizes and volumes of sorbents.

Sorbent	Specific surface area [$m^2\ g^{-1}$]	Average pore size[nm]	$V_{macro+meso}$ [$cm^3\ g^{-1}$]	V_{micro} [$cm^3\ g^{-1}$]
MK	11.5	18.2	0.047	0.005
MK-GP	22.4	31.0	0.165	0.008
BFS	2.79	12.7	0.008	0.001
BFS-GP	64.5	5.93	0.070	0.025
BFS-GP-Ba	63.1	6.32	0.070	0.030

Macropore: $d_0 > 50$ nm, Mesopore: 2 nm $\leq d_0 \leq$ 50 nm, Micropore: $d_0 \leq 2$ nm.

Table 3 shows the chemical composition of BFS, BFS-GP and Ba-BFS-GP. The main components of BFS are calcium, silicon, magnesium, aluminium and sulphur. In addition, sorbents included some other impurities. Aluminium and silicon contents decrease while Na content increases after geopolymerisation. In addition, the loss on ignition (L.O.I.) increases due to the increased water content. The decrease of CaO as BFS is converted into BFS-GP is possibly due to the dissolution of gehlenite and other phases [27]. In Ba-BFS-GP, Na ions are completely replaced by Ba, as signified by corresponding concentrations.

Table 3. Main chemical constituents as determined by XRF.

Composition	BFS [w/w%]	BFS-GP [w/w%]	Ba-BFS-GP [w/w%]
CaO	38.5	29.9	26.3
SiO_2	27.2	25.8	26.8
MgO	9.4	6.4	7.1
Al_2O_3	8.4	5.9	6.7
SO_3	3.8	2.7	0.7

Na_2O	0.3	8.0	0.0
Ba	0.0	0.0	17.3
Other*	2.9	2.4	0.0
L.O.I.	0.5	12.9	14.5
Sum	90.9	93.9	99.4

*Including Ti, Fe_2O_3, K_2O, Mn.

The XRD patterns (Fig. 1) of BFS, BFS-GP, and Ba-BFS-GP indicate initially a completely X-ray amorphous structure, formation of hydrotalcite ($Mg_6Al_2CO_3(OH)_{16}\cdot4(H_2O)$) and haturite ($Ca_3SiO_5$) after geopolymerisation and further formation of witherite ($BaCO_3$) after Ba-modification.

Figure 1. XRD patterns of blast-furnace slag (BFS), blast-furnace-slag geopolymer (BFS-GP) and barium-modified blast-furnace-slag geopolymer (Ba-BFS-GP) samples. HT = hydrotalcite, HAT = haturite, W = witherite.

FTIR spectra for BFS, BFS-GP and Ba-BFS-GP are shown in Fig. 2. The peak in the spectra of Ba-BFS-GP at 856 cm^{-1} is related to the witherite ($BaCO_3$) vibration. The bands in the spectra of BFS, Ba-BFS and Ba-BFS-GP appearing at 960, 942, 894 cm^{-1}, respectively, belong to Si-O stretching vibrations [59]. The bands at 1471 and 1391 cm^{-1} are associated with carbonate vibration in the structure of Ba-BFS-GP and Ba-BFS [26]. Carbon dioxide shows a strong band in the area of 2350 cm^{-1}, and thus the band in Ba-BFS-GP could be related to adsorbed carbon dioxide [60, 61].

Figure 2. The FTIR spectra of blast-furnace slag (BFS), barium-modified blast-furnace-slag (Ba-BFS) and barium-modified blast-furnace-slag geopolymer (Ba-BFS-GP).

3.2 Effect of initial pH and screening of sorbents

The effect of initial pH on the removal of SO_4^{2-} from mine effluent over BFS-GP, Ba-BFS-GP, Ba-MK and Ba-MK-GP is shown in Fig. 3. Sorption efficiency decreases slightly as the initial pH increases from 4 to 10. This may be due to the competition for the sorption sites by OH^- ions at high pH [22, 62]. Ba-BFS-

GP is the most effective sorbent material and it was selected for further study. Sorption efficiency is c.a. 50% at pH range 4–10.

Figure 3. Total SO_4^{2-} removal percent (left, solid lines) and total adsorbed amount (right, dashed lines) versus initial pH on the sorption of SO_4^{2-} from mine effluent. Sorbent dosage: 5 g L^{-1}, contact time: 24 h, temperature: 22–23 °C, adsorbate: mine effluent (C_0, SO_4^{2-}: ~850–870 mg L^{-1}).

3.3 Effect of initial SO_4^{2-} concentration

The effect of initial SO_4^{2-} concentration was investigated with model solutions in the range of 100–1800 mg L^{-1}. The results are presented in Fig. 4. The SO_4^{2-} sorption capacity of Ba-BFS-GP increases as the SO_4^{2-} concentration is increased and reaches a maximum value (90 mg g^{-1}) at about 1200 mg L^{-1}. The initial sharp rise of sorption capacity in Fig. 4 indicates that sorption sites are readily available and the surface becomes saturated as the curve levels off [22, 62].

Figure 4. Effect of the initial concentration on the sorption of SO_4^{2-} on Ba-BFS-GP from model solution. Initial pH: 7–8, sorbent dosage: 5 g L^{-1}, contact time: 24 h, temperature: 22–23 °C.

3.4 Effect of sorbent dosage and temperature

The effect of Ba-BFS-GP dosage on the removal of SO_4^{2-} from model solution and mine effluent are shown in Fig. 5. In both cases the percentage of SO_4^{2-} removal increases with the increasing sorbent dosage and reaches a saturation level at high doses. This phenomenon could be explained by the increase in surface area and the available sorption sites with an increase in the sorbent dosage [63–65]. The sorbent reached maximum removal of SO_4^{2} at dose 10 g L^{-1} of sorbent, probably due to the of mass transfer resistance of SO_4^{2-} from bulk liquid to the surface of the solid, which becomes important at high sorbent loading. In addition, at 40 °C the percentage of SO_4^{2-} removal was decreased slightly with the higher dosage (> 10 g L^{-1}). The higher sorbent dosage results in interference or repulsive forces between binding sites and formation of particle aggregates,

decreasing the interaction of SO_4^{2-} with the sorbent and reducing the total surface area of the sorbent [10, 22, 63–66]. Maximum removal efficiencies with model solution and sorbent dosage 10 g L^{-1} were 68% (51.98 mg g^{-1}), 60% (59.67 mg g^{-1}) and 55% (51.98 mg g^{-1}) at 10, 23 and 40 °C, respectively. In the case of mine effluent, maximum sorption efficiency was 100% (85.69 mg g^{-1}) at 23 °C. The better removal efficiency of SO_4^{2-} in mine effluent compared to model solution could be explained by different initial concentrations and partially by the presence of sodium: sodium hinders SO_4^{2-} removal via the formation of aqueous sodium sulphate complex. The effect of sodium was calculated by MineQL software [67] to account for approximately 10% of the lower removal efficiency.

The sorption capacity (q, mg g^{-1}) increases as temperature is increased (Fig. 5). This indicates that the sorption is an endothermic process in nature. An increase in temperature from 10 °C to 23 °C has a larger effect on sorption capacity than a further increase from 23 °C to 40 °C.

Figure 5. Effect of Ba-BFS-GP dosage on SO_4^{2-} removal. a) Model solution: $C_0(SO_4^{2-})$: ~1200 mg L^{-1}, contact time: 3 h. b) Mine effluent: $C_0(SO_4^{2-})$: 865 mg L^{-1}, contact time: 24 h. In both cases initial pH was 7–8.

3.5 Adsorption isotherms

Bi-Langmuir, Sips, R–P and Toth isotherm models were applied for the experimental results of Ba-BFS-GP (Fig. 6 and Table 4). Comparison of the results for the errors (RMSE, X^2) and correlation coefficients (R^2) indicated that the SO_4^{2-} sorption onto Ba-BFS-GP from model solution can be best represented by the Sips isotherm. Maximum experimental ($q_{m,exp}$) and theoretical ($q_{m,calc}$) sorption capacities are quite similar. In the case of mine effluent, all studied isotherm models gave practically similar correlation coefficient values (R^2: 0.920–0.930) and errors.

Figure 6. Bi-Langmuir, Sips, Redlich-Peterson and Toth isotherms of SO_4^{2-} sorption on Ba-BFS-GP. a) Model solution: $C_0(SO_4^{2-})$: 100–1800 mg L^{-1}, sorbent dose: 5 g L^{-1}. b) Mine effluent: $C_0(SO_4^{2-})$: 865 mg L^{-1}, sorbent dose: 1.3–15 g L^{-1}. Initial pH was 7–8, contact time 24 h and temperature 22–23 °C.

Table 4. Isotherm parameters and errors for the sorption of SO_4^{2-} removal on Ba-BFS-GP.

	Constant (unit)	Model solution[a)]	Mine effluent[b)]
Isotherm			
Experimental	q_m (mg g^{-1})	91.1	119.0
Bi-Langmuir	q_{m1} (mg g^{-1})	42.109	55.290
	b_{L1} (L mg^{-1})	0.463	0.400
	q_{m2} (mg g^{-1})	42.109	55.290
	b_{L2} (L mg^{-1})	0.463	0.400
	R^2	0.926	0.920
	RMSE	8.737	10.452
	X^2	3.810	7.501
Sips	q_{Sm} (mg g^{-1})	83.691	110.580
	b_S (L mg^{-1})	0.482	0.400
	n_S	2.102	1.000
	R^2	0.951	0.920
	RMSE	6.174	9.541
	X^2	1.822	7.501
Redlich-Peterson (R–P)	K_R (dm^3 g^{-1})	48.978	57.107
	a_R (dm^3 mg^{-1})	0.734	0.650
	β	0.964	0.963
	R^2	0.931	0.929
	RMSE	7.318	8.945
	X^2	3.990	7.714
Toth	q_{Th} (mg g^{-1})	64.937	85.863
	K_{Th} (mg dm^{-3})Th	1.391	1.593
	Th	1.042	1.043
	R^2	0.932	0.930
	RMSE	7.257	8.870
	X^2	3.943	7.071

a) Model solution: Initial pH: 7–8, $C_o(SO_4^{2-})$: 100–1800 mg L^{-1}, m(Ba-BFS-GP): 5 g L^{-1}.
b) Mine effluent: Initial pH: 7–8, $C_o(SO_4^{2-})$: 865 mg L^{-1}, m(Ba-BFS-GP): 1.3–15 g L^{-1}.
Contact time: 24 h and temperature 22–23 °C.

The sorbents produced were compared with other materials (Table 5). The Ba-BFS-GP shows a higher or comparable sorption capacity to other similar anion sorbents.

Table 5. Comparison of adsorption capacity q_m(mg g^{-1}) of various sorbents for the removal of SO_4^{2-} from aqueous phase.

Sorbent	Capacity q (mg g^{-1})	pH	Concentration (mg L^{-1})	Reference
Coir pith carbon	0.06[a]	4.0	20–80	[68]
Iron sand	1.15[b] (12 mmol g^{-1})	-	20–2000	[15]
Feldspar	0.275[a]	5.5	1–5	[5]
Pulp and paper waste	2.786[b] (29 mmol g^{-1})	-	20–2000	[15]
Surfactant-modified palygorskite	3.24[b]	4.0	20–130	[4]
$ZnCl_2$ activated coir pith carbon	4.9[a]	4.0	20–80	[68]
Surfactant-modified clinoptilolite	~ 7.0[a]	-	96–500	[20]
ɣ-Al_2O_3	7.7[a]	5.7	20–40	[69]
Surfactant modified coir pith	8.76[a]	2	10–50	[7]
Raw rice straw	11.68[a]	6.4	50–500	[1]
Flotation fines	21.23[b] (221 mmol g^{-1})	-	20–2000	[15]
Limestone	23.7[a]	9.6–9.8	588–1100	[2]
Filter sand	25.07[b] (261 mmol g^{-1})	-	20–2000	[15]
Alkali-treated fly ash	43.0[a]	-	200	[36]
Ba-modified zeolite	64.10[a] (1.33 meq g^{-1})	6.0	<1000	[21]
Epichlorohydrin and trimethylamine modified rice straw	74.76[a]	6.4	50–500	[1]
poly(*m*-phenylenediamine)	108.5[a]	1.75–3	50–4000	[11]
Ba-modified blast-furnace-slag geopolymer	119.0[b]	7–8	865	This study
Chitin-based shrimp shells	156.0[a]	4.5	2350	[70]

[a]Langmuir maximum sorption capacity, $q_{m,calc}$, [b]Experimental maximum sorption capacity

3.6 Effect of contact time

The effect of contact time on the removal of SO_4^{2-} by Ba-BFS-GP at room temperature is presented in Fig. 7. It can be seen from the curves that the sorption is rapid in the first 10 min while sorption equilibrium is attained at approximately 3 h. The rate of SO_4^{2-} removal was higher at the beginning of the sorption experiment due to a larger number of available adsorption sites [71]. Maximum SO_4^{2-} sorption capacities of Ba-BFS-GP were 159.1 mg g^{-1} (74.5% removal) and 99.0 mg g^{-1} (58.0% removal) in model SO_4^{2-} solution and mine effluent, respectively.

Figure 7. Effect of contact time on the removal efficiency of SO_4^{2-} onto Ba-BFS-GP. o: Model SO_4^{2-} solution (C_0, SO_4^{2-}: 1100 mg L^{-1}), □: Mine effluent (C_0, SO_4^{2-}: 853 mg L^{-1}). Initial pH: 7–8, sorbent dosage: 5 g L^{-1}, temperature: 22–23 °C.

3.7 Kinetic modelling

The pseudo-first-order, pseudo-second-order and Elovich kinetic models were used to evaluate the experimental data. The results are shown in Fig. 8, and the corresponding kinetic parameters are listed in Table 6. The best fit was observed with the pseudo-second-order kinetic model. Theoretical $q_{e,cal}$ values of the pseudo-second-order kinetic model agree well with the experimental uptake values.

Figure 8. a) Pseudo-first-order kinetic, b) pseudo-second-order kinetic and c) Elovich model plots of SO_4^{2-} sorption on Ba-BFS-GP. o: Model SO_4^{2-} solution (C_0, SO_4^{2-}: 1100 mg L^{-1}), □: Mine effluent (C_0, SO_4^{2-}: 853 mg L^{-1}). Initial pH: 7–8, sorbent dosage: 5 g L^{-1}, contact time: 24 h, temperature: 22–23 °C.

Table 6. Pseudo-first-order, pseudo-second-order and Elovich model parameters for Ba-BFS-GP in SO_4^{2-} removal.

Pseudo-first-order model				
C_0 (mg L^{-1})	$q_{e,exp}$ (mg g^{-1})	$q_{e,calc}$ (mg g^{-1})	k_1 (min^{-1})	R^2
1100	159.08	40.51	0.0108	0.9776
853	99.0	56.65	0.0085	0.9643
Pseudo-second-order				
C_0 (mg L^{-1})	$q_{e,exp}$ (mg g^{-1})	q_{calc} (mg g^{-1})	k_2 (g mg^{-1} min^{-1})	R^2
1100	159.08	158.73	2.217E-03	1
853	99.0	100	7.6E-04	0.9994
Elovich model				
C_0 (mg L^{-1})	$q_{e,exp}$ (mg g^{-1})	b (g L^{-1})	υ_0 (mg g^{-1} min^{-1})	R^2
1100	159.08	0.1633	1E+09	0.9214
853	99.0	0.1037	224.175	0.8826

3.8 Weber and Morris intraparticle diffusion model

The Weber and Morris intraparticle diffusion model was applied to the kinetic data of Ba-BFS-GP against the SO_4^{2-} (Fig. 9). If a plot of q_t versus $t^{1/2}$ presents a straight line from the origin, the rate-limiting step in the sorption mechanism is diffusion from the outer surface into the pores of the material. The data of SO_4^{2-} sorption on Ba-BFS-GP shows two plots, which do not pass through the origin. This indicates that intraparticle diffusion is not the rate-limiting step. The first stage can be attributed to the instantaneous or external surface sorption while the second stage is the low diffusion of adsorbate from the surface to the inner pore [62].

Figure 9. Weber and Morris intraparticle diffusion model plot of SO_4^{2-} sorption on Ba-BFS-GP. o: Model SO_4^{2-} solution (C_0, SO_4^{2-}: 1100 mg L^{-1}), □: Mine effluent (C_0, SO_4^{2-}: 853 mg L^{-1}). Initial pH: 7–8, sorbent dosage: 5 g L^{-1}, contact time: 24 h, temperature: 22–23 °C.

3.9 Thermodynamic parameters

Standard enthalpy (ΔH) and entropy (ΔS) were obtained from the slope and intercept of the plot of ln K_c vs. $1/T$, as shown in Fig. 10 and listed in Table 7. The negative value of ΔG indicated that the sorption process is spontaneous in nature. Affinity of the Ba-BFS-GP for SO_4^{2-} is represented by the positive value of ΔS, which indicated that the sorption process increased the entropy at the solid/solution interface during the sorption process. The positive value of ΔH suggested that the interaction of SO_4^{2-} and Ba-BFS-GP is endothermic in nature. The ΔH obtained from thermodynamic calculations (≤ 40 kJ mol^{-1}) suggests a physisorption process involving weak interactions. [10, 62, 66, 72–74]

Figure 10. Van't Hoff plot for adsorption of SO_4^{2-} removal. Initial pH: 7–8, adsorbent dosage: 5 g L^{-1}, $C_0(SO_4^{2-})$: 1200 mg L^{-1}.

Table 7. Thermodynamics parameters for the sorption of SO_4^{2-} on Ba-BFS-GP at different temperatures.

Temperature (°C)	ΔG(kJ mol^{-1})	ΔS(J mol^{-1} K^{-1})	ΔH(kJ mol^{-1})
10	-10.354		
22	-11.389	56.598	5.556
40	-12.059		

3.10 Column studies

Column studies (Fig. 11) have been carried out for Ba-BFS-GP as a sorbent in order to study its sorption capacity in dynamic conditions. Flow rates of 0.24 and 0.85 L h^{-1} were used for the break-through simulation. Initially, total SO_4^{2-} removal was observed with a lower flow rate. However, the removal of SO_4^{2-} starts to linearly decrease after 40 min (corresponding to 0.16 L of treated effluent) and drops below 50% after 140 min (corresponding to 0.56 L of treated effluent). Therefore, it could be estimated that 18.7 m^3 of mine effluent with a similar composition could be treated with 1 t of Ba-

BFS-GP with over 50% SO_4^{2-} removal. After use, Ba-BFS-GP could be further utilised in selective radium adsorption from contaminated waters due to accumulation of $BaSO_4$ as indicated by Kunze et al. [75]

Figure 11. Breakthrough curves of SO_4^{2-} by Ba-BFS-GP packed column for two different flow rates.

3.11 Barium leaching

The leaching of Ba from Ba-BFS-GP was studied in mine effluent and distilled water at initial pH values of 2 and 8. The results indicate that dissolved Ba^{2+} concentrations from Ba-BFS-GP were 600 and 32 mg L^{-1} at initial pH values 2 and 8 in distilled water. However, in the case of mine effluent ($C_0(SO_4^{-2})$: 850–870 mg L^{-1}) , the dissolved Ba^{2+} concentrations were 0.175 and 0.375 mg L^{-1} at initial pH values 2 and 8, respectively. Clearly lower concentrations of dissolved Ba in mine effluent are due to the instantaneous precipitation of low solubility $BaSO_4$. The limit for Ba content in domestic water is 0.7 mg L^{-1} [76], so it would be safe to utilise Ba-BFS-GP for treating industrial wastewater containing SO_4^{2-}.

3.12 Sorption mechanism

The sorption mechanism of geopolymers in the removal of cations from aqueous solutions has been suggested to be cation exchange [31, 44, 77]. However, geopolymers have low affinity towards sorption of anions due to negative zeta potential [46]. In the present work, geopolymers were converted into Ba-form by a cation-exchange process and further applied for SO_4^{2-} removal. The probable removal mechanism of SO_4^{2-} is based on the surface complexation or precipitation of extremely low solubility $BaSO_4$ (K_{sp} = 1.08 * 10^{-10} at 25°C, solubility 0.0031 g L^{-1}, 20°C) [50, 78]. Due to the low solubility, $BaSO_4$ is considered non-toxic. However, the removal of sulphate with the direct precipitation as $BaSO_4$ is not recommended due to generation of secondary waste in the form of sludge [14]. The presence of $BaSO_4$ was confirmed with XRD from a used sorbent material.

4 Conclusions

Ba-modified blast-furnace-slag and Ba-modified metakaolin with and without a geopolymerisation step were studied for SO_4^{2-} removal. Ba-modified geopolymerised materials exhibit higher SO_4^{2-} ion removal capacity than Ba-modified materials without a geopolymerisation step. This is explained by the cation exchange process (Na^+ is replaced by Ba^{2+}) taking place in the geopolymer framework structure during Ba-modification. The best sorbent material for SO_4^{2-} removal was Ba-BFS-GP. The optimum pH required for maximum sorption was found to be 7–8. The maximum experimental sorption capacities were 91.1 and 119.0 mg g^{-1} for synthetic model solution and mine effluent, respectively. Sorption capacities found in this study were among the highest of reported in the literature. The Sips isotherm model described the sorption well. Sorption kinetics followed the pseudo-second-order kinetic model, and the Weber and Morris intraparticle diffusion model showed that the sorption mechanism included two different steps. The positive enthalpy value indicates that the adsorption process was endothermic in nature. The results from the present study indicate that Ba-BFS-GP could be a technically feasible SO_4^{2-} sorbent for wastewater treatment (e.g. in the mining industry) especially for applications in which very low SO_4^{2-} levels are desired.

Acknowledgments

This study was conducted as a part of SULKA (A32164, 524/2012) and GeoSorbents (Tekes, project 4684/31/2014) projects. Maa- ja vesitekniikan tuki ry. is gratefully acknowledged for funding this study. The authors would like to thank MSc Sara Lopéz and BSc Riikka Juhola for their contribution in some laboratory experiments and Mr. Jaakko Pulkkinen and Mr. Tuomo Vähätiitto for their assistance in SO_4^{2-} and metal analysis.

References

[1] W. Cao, Z. Dang, X. Zhou, X. Yi, P. Wu, N. Zhu, G. Lu, Removal of sulphate from aqueous solution using modified rice straw: Preparation, characterization and adsorption performance, Carbohydr. Polym. 85 (2011) 571–577.

[2] A.M. Silva, R.M.F. Lima, V.A. Leão, Mine water treatment with limestone for sulfate removal, J. Hazard. Mater. 221–222 (2012) 45–55.

[3] D. Rui, L. Yuanfa, W. Xingguo, H. Jianhua, Adsorption of sulfate ions from aqueous solution by surfactant-modified palygorskite, J. Chem. Eng. Data. 56 (2011) 3890–3896.

[4] N. Priyantha, S. Perera, Removal of sulfate, phosphate and colored substances in wastewater effluents using feldspar, Water Res. Manage. 14 (2000) 417–433.

[5] Finlex, Ministry of Social Affairs and Health, 1352/2015 Sosiaali- ja terveysministeriön asetus talousveden laatuvaatimuksista ja valvontatutkimuksista (In Finnish), http://www.finlex.fi, 2015 (accessed 01.12.15).

[6] C. Namasivayam, M.V. Sureshkumar, Removal of sulfate from water and wastewater by surfactant-modified coir pith, an agricultural solid "waste" by adsorption methodology, J. Env. Eng. Manage. 17 (2007) 129–135.

[7] INAP, Treatment of sulphate in mine effluents, International network for acid prevention. Available from http://www.inap.com.au/public_downloads/Research_Projects/Treatment_of_Sulphate_in_Mine_Effluents_-_Lorax_Report.pdf, 2003 (accessed 01.12.15).

[8] L. Hartinger, Handbook of effluent treatment and recycling for the metal finishing industry, 2. ed., ASM International, Novelty, OH, USA, 1994.

[9] A.J. Geldenhuys, J.P. Maree, M. de Beer, P. Hlabela, An integrated limestone/lime process for partial sulphate removal, J. S. Afr. Inst. Min. Metall. 103 (2003) 345–354.

[10] R. Katal, M.S. Baei, H.T. Rahmati, H. Esfandian, Kinetic, isotherm and thermodynamic study of nitrate adsorption from aqueous solution using modified rice husk, J. Ind. Eng. Chem. 18 (2012) 295–302.

[11] P. Sang, Y. Wang, L. Zhang, L. Chai, H. Wang, Effective adsorption of sulfate ions with poly(m-phenylenediamine) in aqueous solution and its adsorption mechanism, Transactions of Nonferrous Metals Society of China. 23 (2013) 243–252.

[12] A.C.A. de Lima, R.F. Nascimento, F.F. de Sousa, J.M. Filho, A.C. Oliveira, Modified coconut shell fibers: A green and economical sorbent for the removal of anions from aqueous solutions, Chem. Eng. J. 185–186 (2012) 274–284.

[13] M.S. Salman, Removal of sulfate from waste water by activated carbon, Al-Khwarizmi Eng. J. 5 (2009) 72–76.

[14] N. Koshy, D.N. Singh, Fly ash zeolites for water treatment applications. J. Environ. Chem. Eng. 4 (2016) 1460–1472.

[15] E. Iakovleva, E. Mäkilä, J. Salonen, M. Sitarz, M. Sillanpää, Industrial products and wastes as adsorbents for sulphate and chloride removal from synthetic alkaline solution and mine process water. Chem. Eng. J. 259 (2015) 364–371.

[16] R. Juang, W. Wu, Adsorption of sulfate and copper(II) on goethite in relation to the changes of zeta potentials, J. Colloid Interface Sci. 249 (2002) 22–29.

[17] P. Roonasi, A. Holmgren, An ATR-FTIR study of sulphate sorption on magnetite; rate of adsorption, surface speciation, and effect of calcium ions, J. Colloid Interface Sci. 333 (2009) 27–32.

[18] R.P.J.J. Rietra, T. Hiemstra, W.H. van Riemsdijk, Comparison of selenate and sulfate adsorption on goethite, J. Colloid Interface Sci. 240 (2001) 384–390.

[19] A.M. Jubb, D. Verreault, R. Posner, L.J. Criscenti, L.E. Katz, H.C. Allen, Sulfate adsorption at the buried hematite/solution interface investigated using total internal reflection (TIR)-Raman spectroscopy, J. Colloid Interface Sci. 400 (2013) 140–146.

[20] A.D. Vujaković, M.R. Tomašević-Čanović, A.S. Daković, V.T. Dondur, The adsorption of sulphate, hydrogenchromate and dihydrogenphosphate anions on surfactant-modified clinoptilolite, Appl. Clay. Sci. 17 (2000) 265–277.

[21] C.R. Oliveira, J. Rubio, New basis for adsorption of ionic pollutants onto modified zeolites, Min. Eng. 20 (2007) 552–558.

[22] R. Katal, M. Vafaie Sefti, M. Jafari, A.H. Saeedi Dehaghani, S. Sharifian, M.A. Ghayyem, Study effect of different parameters on the sulphate sorption onto nano alumina, J. Ind. Eng. Chem. 18 (2012) 230–236.

[23] T. Delfosse, P. Delmelle, B. Delvaux, Sulphate sorption at high equilibrium concentration in Andosols, Geoderma. 136 (2006) 716–722.

[24] F. Bazer-Bachi, M. Descostes, E. Tevissen, P. Meier, B. Grenut, M.-. Simonnot, M. Sardin, Characterization of sulphate sorption on Callovo-Oxfordian argillites by batch, column and through-diffusion experiments, Physics and Chemistry of the Earth, Parts A/B/C. 32 (2007) 552–558.

[25] J.P. Gustafsson, M. Akram, C. Tiberg, Predicting sulphate adsorption/desorption in forest soils: Evaluation of an extended Freundlich equation, Chemosphere. 119 (2015) 83–89.

[26] V.F.F. Barbosa, K.J.D. MacKenzie, C. Thaumaturgo, Synthesis and characterisation of materials based on inorganic polymers of alumina and silica: sodium polysialate polymers, Int. J. Inorg. Mat. 2 (2000) 309–317.

[27] S.V. Dimitrova, D.R. Mehanjiev, Interaction of blast-furnace slag with heavy metal ions in water solutions, Wat. Res. 34 (2000) 1957–1961.

[28] P. Duxson, A. Fernández-Jiménez, J. L. Provis, G. C. Lukey, A. Palomo, J.S.J. van Deventer, Geopolymer technology: the current state of the art, J. Mater. Sci. (2007) 42:2917–2933.

[29] L. Li, S. Wang, Z. Zhu, Geopolymeric adsorbents from fly ash for dye removal from aqueous solution, J. Colloid Interface Sci. 300 (2006) 52–59.

[30] Q. Tang, Y. Ge, K. Wang, Y. He, X. Cui, Preparation and characterization of porous metakaolin-based inorganic polymer spheres as an adsorbent, Mater Des. 88 (2015) 1244–1249.

[31] S.J. O'Connor, K.J.D. MacKenzie, M.E. Smith, J.V. Hanna, Ion exchange in the charge-balancing sites of aluminosilicate inorganic polymers, J. Mater. Chem. 20 (2010) 10234–10240.

[32] F.J. López, S. Sugita, M. Tagaya, T. Kobayashi, Metakaolin-based geopolymers for targeted adsorbents to heavy metal ion separation. J. Mat. Sci. Chem. Eng. 2 (2014) 16–27.

[33] T.W. Cheng, M.L. Lee, M.S. Ko, T.H. Ueng, S.F. Yang, The heavy metal adsorption characteristics on metakaolin-based geopolymer, Appl. Clay. Sci. 56 (2012) 90–96.

[34] Y.J. Zhang, L.C. Liu, L.L. Ni, B.L. Wang, A facile and low-cost synthesis of granulated blast furnace slag-based cementitious material coupled with Fe_2O_3 catalyst for treatment of dye wastewater, Applied Catalysis B: Environmental. 138–139 (2013) 9–16.

[35] K. Al-Zboon, M.S. Al-Harahsheh, F.B. Hani, Fly ash-based geopolymer for Pb removal from aqueous solution, J. Hazard. Mater. 188 (2011) 414–421.

[36] C.K. Geethamani, S.T. Ramesh, R. Gandhimathi, P.V. Nidheesh, Alkali-treated fly ash for the removal of fluoride from aqueous solutions, Desalination and Water Treatment. 52 (2014) 3466–3476.

[37] N. Koshy, D.N. Singh, B. Jha, S. Kadali, J. Patil, Characterization of Na and Ca zeolites synthesized by various hydrothermal treatments of fly ash. Adv. Civil Eng. Mat. ASTM International. 4 (2015) 131–143.

[38] S. Wang, L. Li, Z.H. Zhu, Solid-state conversion of fly ash to effective adsorbents for Cu removal from wastewater, J. Hazard. Mater. 139 (2007) 254–259

[39] S. Andrejkovičová, A. Sudagar, J. Rocha, C. Patinha, W. Hajjaji, E. Ferreira da Silva, A. Velosa, F. Rocha, The effect of natural zeolite on microstructure, mechanical and heavy metals adsorption properties of metakaolin based geopolymers, Appl. Clay Sci. 126 (2016) 141–152.

[40] G. Gong, S. Ye, Y. Tian, Q. Wang, J. Ni, Y. Chen, Preparation of a new sorbent with hydrated lime and blast furnace slag for phosphorus removal from aqueous solution, J. Haz. Mat. 166 (2009) 714–719.

[41] J. Davidovits, Geopolymers: inorganic polymeric new materials, J. Therm. Anal. 37 (1991) 1633–1656.

[42] J. Davidovits, Geopolymers and geopolymeric new material, J. Thermal. Anal. 35 (1998) 429–441.

[43] R.I. Yousef, B. El-Eswed, M. Alshaaer, F. Khalili, H. Khoury, The influence of using Jordanian natural zeolite on the adsorption, physical, and mechanical properties of geopolymers products, J. Hazard. Mater. 165 (2009) 379–387.

[44] T. Luukkonen, H. Runtti, M. Niskanen, E. Tolonen, M. Sarkkinen, K. Kemppainen, J. Rämö, U. Lassi, Simultaneous removal of Ni(II), As(III), and Sb(III) from spiked mine effluent with metakaolin and blast-furnace-slag geopolymers, J. Environ. Manage. 166 (2016) 579–588.

[45] T.W. Chen, M.L. Lee, M.S. Ko, T.H. Ueng, S.F. Yang, The heavy metal adsorption characteristics on metakaolin-based geopolymer, Appl. Clay. Sci. 56 (2012) 90–96.

[46] T. Luukkonen, M. Sarkkinen, K. Kemppainen, J. Rämö, U. Lassi, Metakaolin geopolymer characterization and application for ammonium removal from model solutions and landfill leachate, Appl. Clay. Sci. 119, Part 2 (2016) 266–276.

[47] Š. C. Stefanović, N. Z. Logar, K. Margeta, N. N. Tušar, I. Arčon, K. Maver, J. Kovač, V. Kaučič, Structural investigation of Zn^{2+} sorption on clinoptilolite tuff from the Vranjska Banja deposit in Serbia, Micropor. Mesopor. Mater. 105 (2007) 251–259.

[48] C.R. Oliveira, J. Rubio, New basis for adsorption of ionic pollutants onto modified zeolites, Min. Eng. 20 (2007) 552–558.

[49] M. Šiljeg, Š. C. Stefanović, M. Mazaj, N. N. Tušar, I. Arčon, J. Kovač, K. Margeta, V. Kaučič, N. Z. Logar, Structure investigation of As(III)- and As(V)-species bound to Fe-modified clinoptilolite tuffs, Micropor. Mesopor. Mat. 118 (2009) 408–415.

[50] K. Margeta, N. Z. Logar, M. Šiljeg, A. Farkaš, Natural zeolites in water treatment - How effective is their use, http://dx.doi.org/10.5772/50738

[51] D. Graham, The characterization of physical adsorption systems. I. The equilibrium function and standard free energy of adsorption, J. Phys. Chem. 57 (1953) 665–669.

[52] R. Sips, On the structure of a catalyst surface, J. Chem. Phys. 16 (1948) 490–495.

[53] O. Redlich, DL Peterson, A useful adsorption isotherm. J. Phys. Chem. 63 (1959) 1024–1024.

[54] J. Toth, State equations of the solid gas interface layer, Acta Chem. Acad. Hung. 69 (1971) 311–328.

[55] S. Lagergren, About the theory of so-called adsorption of soluble substances., K. Sven. Vetenskapsakad. Handl. 24 (1898) 1–39.

[56] Y.S. Ho, G. McKay, Pseudo-second order model for sorption processes, Process Biochemistry. 34 (1999) 451–465.

[57] J. Zeldowitsch, Über den mechanismus der katalytischen oxydation von CO an MnO_2 [About the mechanism of catalytic oxidation of CO over MnO_2], Acta Physicochim. URSS. 1 (1934) 364–449.

[58] W.J. Weber Jr., J.C. Morris, Kinetics of adsorption of carbon from solution, J. Sanit. Eng. Div. Am. Soc. Civ. Eng. 89 (1963) 31–60.

[59] M.A. Karakassides, D. Gournis, D. Petridis, An infrared reflectance study of Si-O vibrations in thermally treated alkali-saturated montmorillonates, Clay Minerals. 38 (1999) 429–438.

[60] C.O. Arean, G.F. Bibiloni, M.R. Delgado, FT-IR spectroscopic and thermodynamic study on the adsorption of carbon dioxide and dinitrogen in the alkaline zeolite K-L, Appl. Surf. Sci. 259 (2012) 367–370.

[61] K. Tan, S. Zuluaga, Q. Gong, Y. Gao, N. Nijem, J. Li, T. Thonhauser, Y.J. Chabal, Competitive co-adsorption of CO_2 with H_2O, NH_3, SO_2, NO, NO_2, N_2, O_2, and CH_4 in M-MOF-74 (M= Mg, Co, Ni): the role of hydrogen bonding, Chem. Mater. 27 (2015) 2203–2217.

[62] A. Bhatnagar, E. Kumar, M. Sillanpää, Nitrate removal from water by nano-alumina: Characterization and sorption studies, Chem. Eng. J. 163 (2010) 317–323.

[63] M. Özacar, I.A. Sengil, Adsorption of metal complex dyes from aqueous solutions by pine sawdust, Bioresour. Technol. 96 (2005) 791–795.

[64] A. Shukla, Y. Zhang, P. Dubey, J.L. Margrave, S.S. Shukla, The role of sawdust in the removal of unwanted materials from water, J. Hazard. Mater. 95 (2002) 137–152.

[65] D.H. Lataye, I.M. Mishra, I.D. Mall, Adsorption of α-picoline onto rice husk ash and granular activated carbon from aqueous solution: Equilibrium and thermodynamic study, Chem. Eng. J. 147 (2009) 139–149.

[66] N.Y. Mezenner, A. Bensmaili, Kinetics and thermodynamic study of phosphate adsorption on iron hydroxide-eggshell waste, Chem. Eng. J. 147 (2009) 87–96.

[67] W.D. Schecker, D.C. McAvoy, MINEQL+ a chemical equilibrium modelling system version 4.5 for windows. User's Manual. Environmental research software, 2003.

[68] C. Namasivayam, D. Sangeetha, Application of coconut coir pith for the removal of sulfate and other anions from water, Desalination. 219 (2008) 1–13.

[69] C. Wu, C. Kuo, C. Lin, S. Lo, Modeling competitive adsorption of molybdate, sulfate, selenate, and selenite using a Freundlich-type multi-component isotherm, Chemosphere. 47 (2002) 283–292.

[70] A. Moret, J. Rubio, Sulphate and molybdate ions uptake by chitin-based shrimp shells, Minerals Eng. 16 (2003) 715–722.

[71] E.-.Z. El-Ashtoukhy, N.K. Amin, O. Abdelwahab, Removal of lead (II) and copper (II) from aqueous solution using pomegranate peel as a new adsorbent, Desalination. 223 (2008) 162–173.

[72] A. Bhatnagar, A.K. Minocha, M. Sillanpää, Adsorptive removal of cobalt from aqueous solution by utilizing lemon peel as biosorbent, Biochem. Eng. J. 48 (2010) 181–186.

[73] H. Kalavathy, B. Karthik, L.R. Miranda, Removal and recovery of Ni and Zn from aqueous solution using activated carbon from Hevea brasiliensis: Batch and column studies, Colloids and Surfaces B: Biointerfaces. 78 (2010) 291–302.

[74] M.V. Subbaiah, Y.S. Yun, Biosorption of nickel(II) from aqueous solution by the fungal mat of trametes versicolor (Rainbow) biomass: equilibrium, kinetics, and thermodynamis studies, Biotechnol. Bioprocess Eng. 18 (2013) 280–288.

[75] C.E. Kunze, I. Hermann, I. Griebel, G. Kiessig, F. Dullies, M. Schreiter, Entwicklung und praxiseinsatz eines hocheffizienten selektiven sorbens fur radium [Development and practical application of a highly selective sorbent for radium. In German, GWF Wasser Abwasser. 143 (2002) Jg., no 7/8.

[76] WHO (2004) Barium in Drinking-water Background document for development of WHO Guidelines for Drinking-water Quality. WHO/SDE/WSH/03.04/76.

URI:http://www.who.int/water_sanitation_health/dwq/chemicals/barium.pdf. Cited 2016/02/01.

[77] T. Skorina, Ion exchange in amorphous alkali-activated aluminosilicates: Potassium based geopolymers, Appl. Clay. Sci. 87 (2014) 205–211.

[78] D.R. Lide, CRC Handbook of Chemistry and Physics. 84. ed., CRC Press, 2003

Graphical Abstract

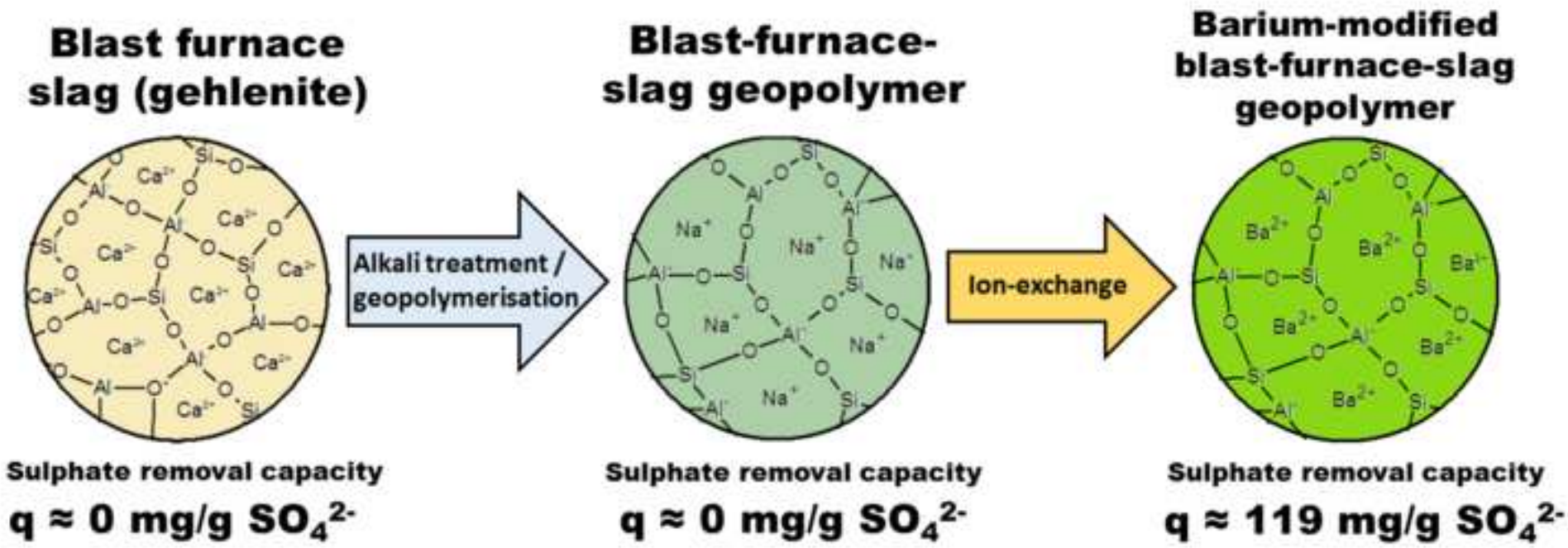

Figure 1

Click here to download high resolution image

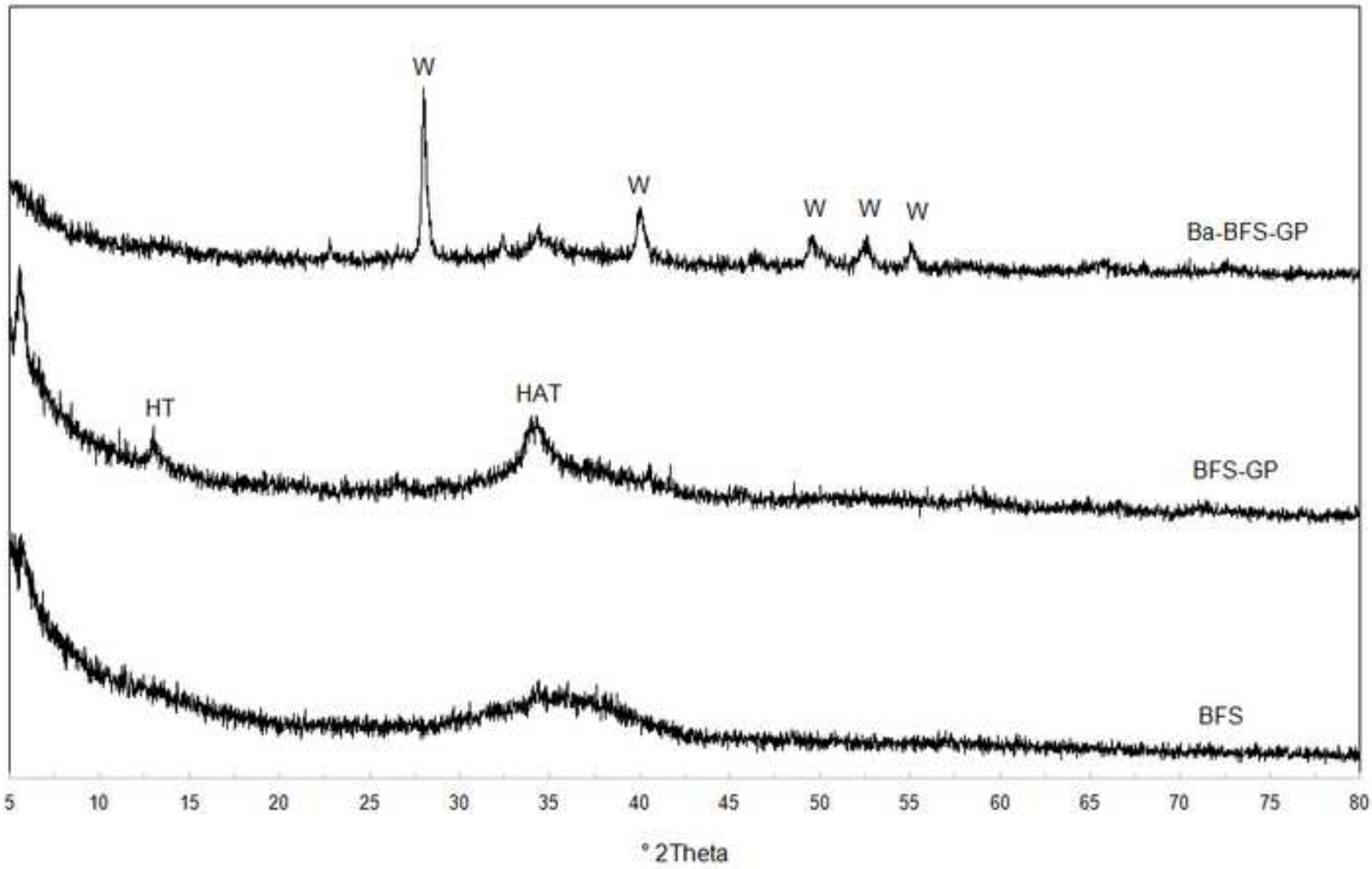

Figure 2

Click here to download high resolution image

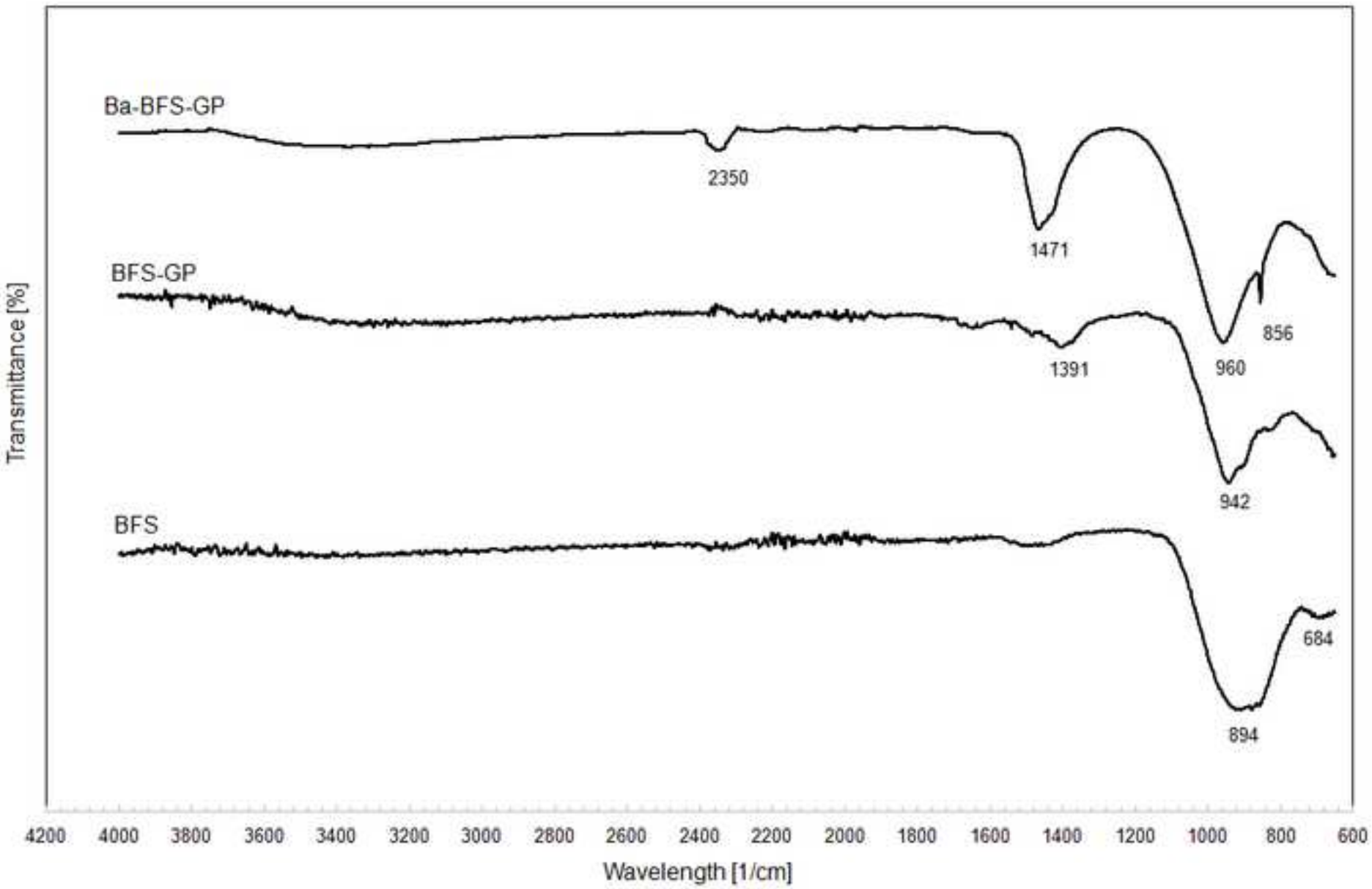

Figure 3

Click here to download high resolution image

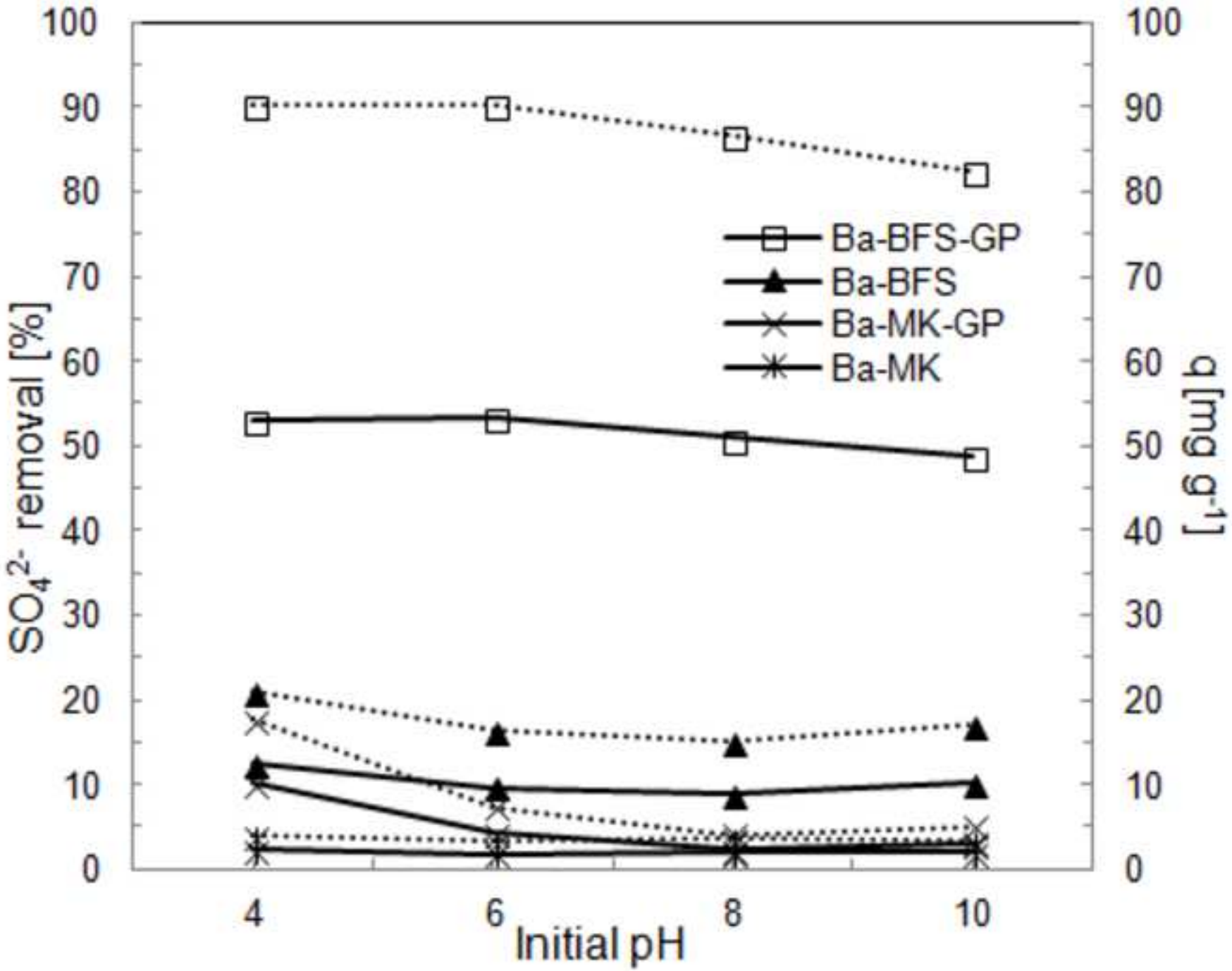

Figure 4

Click here to download high resolution image

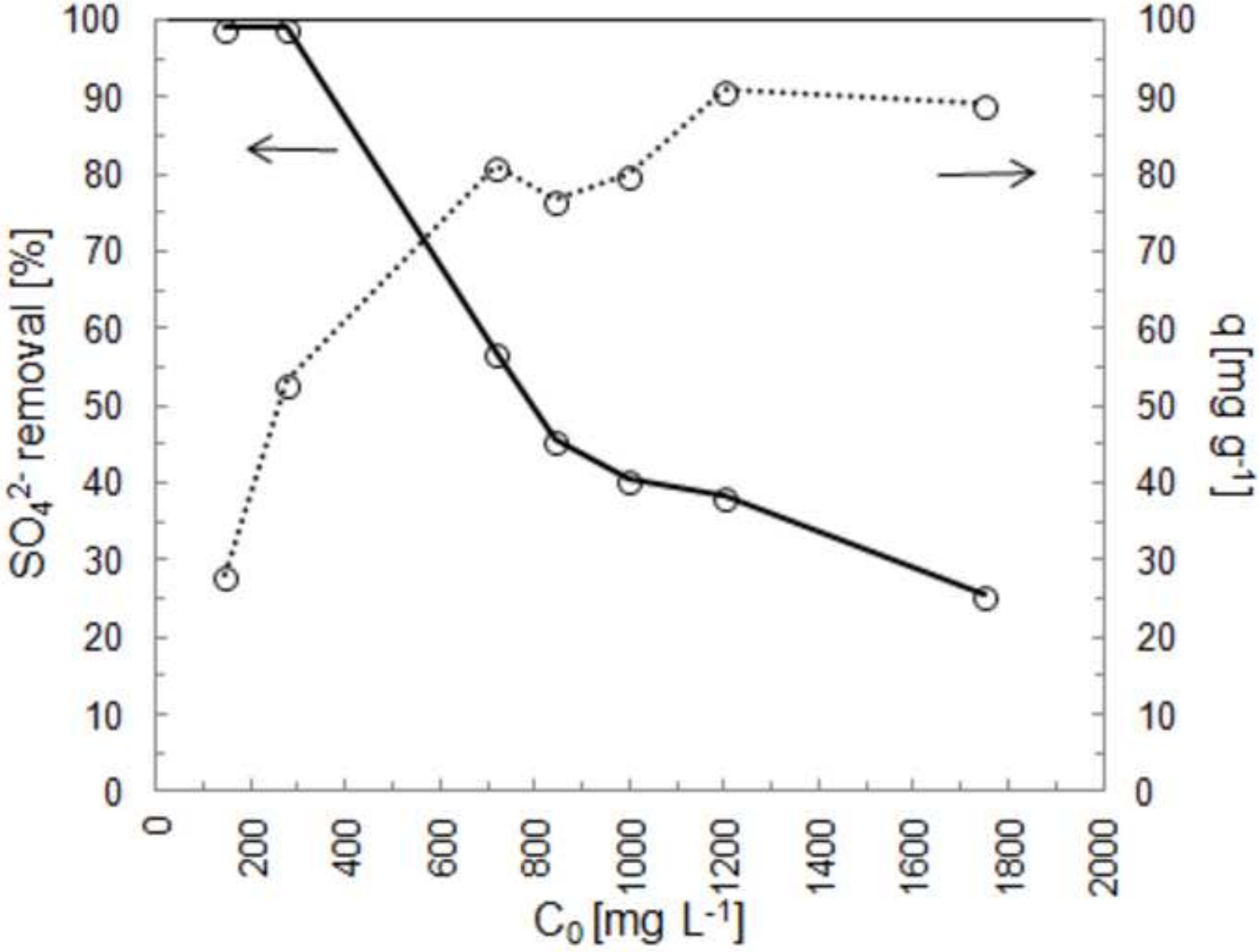

Figure 5 modified

Click here to download high resolution image

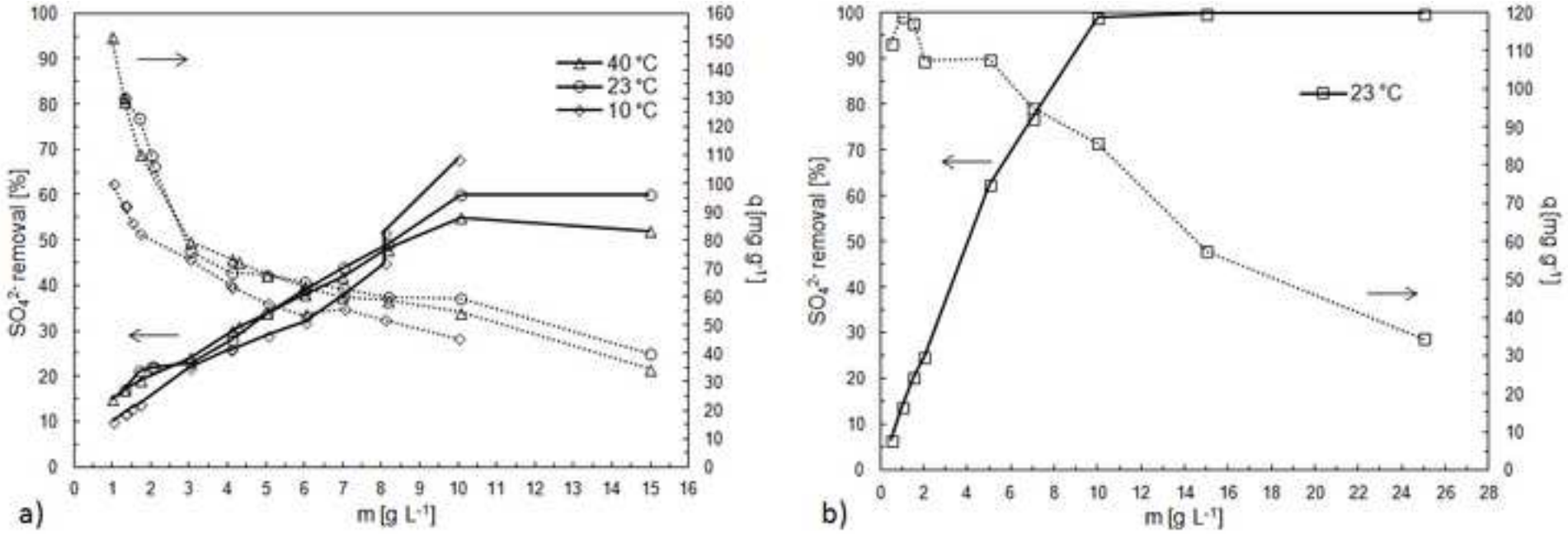

Figure 6

Click here to download high resolution image

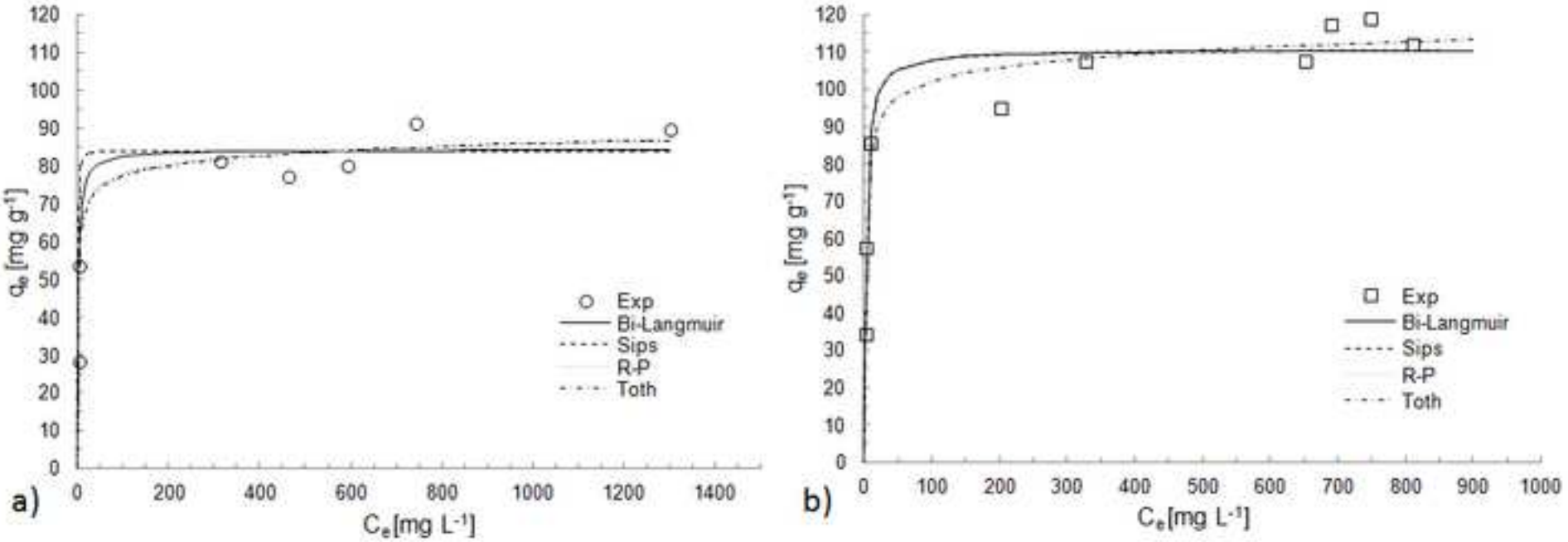

Figure 7 modified

Click here to download high resolution image

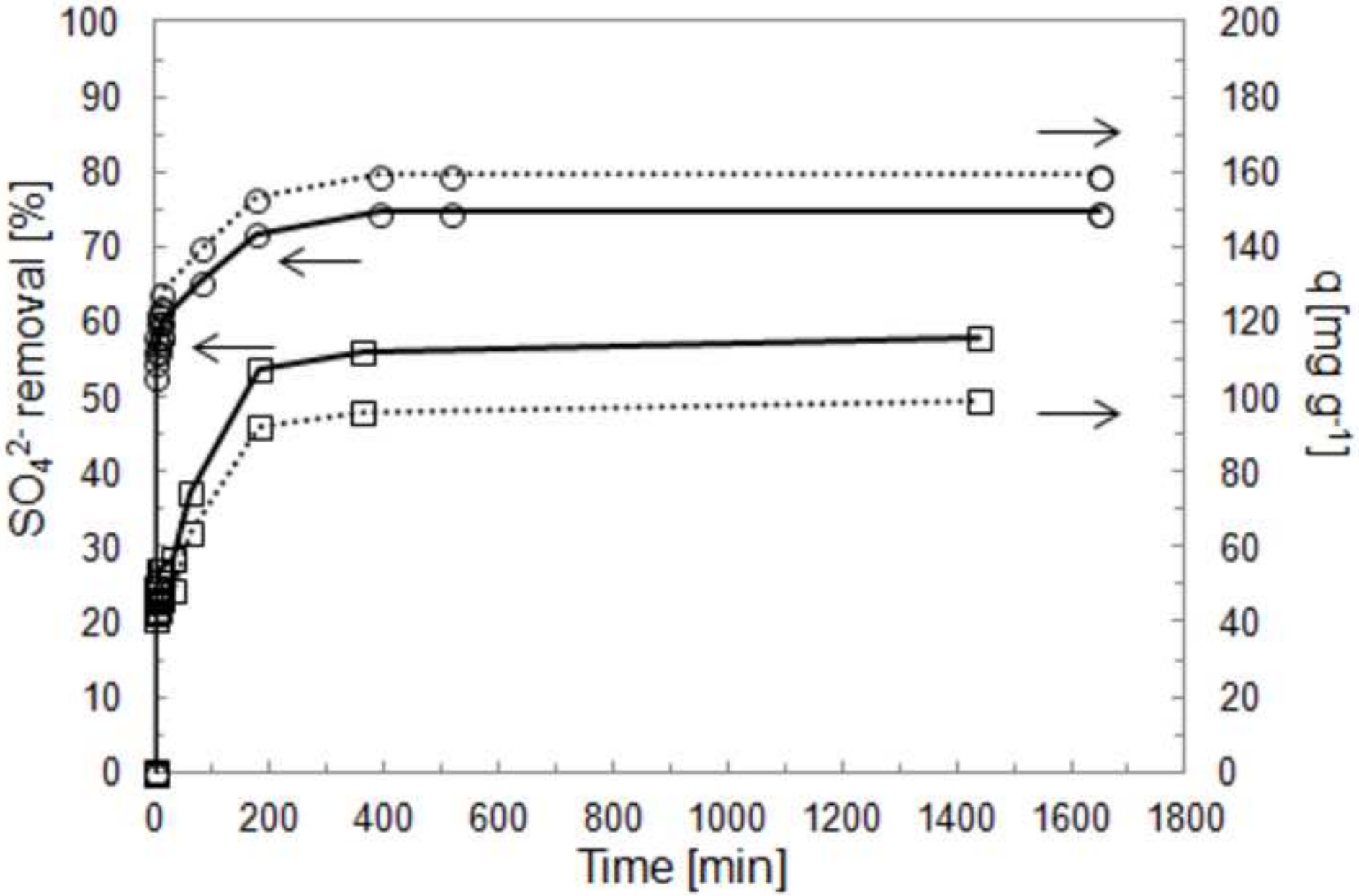

Figure 8

Click here to download high resolution image

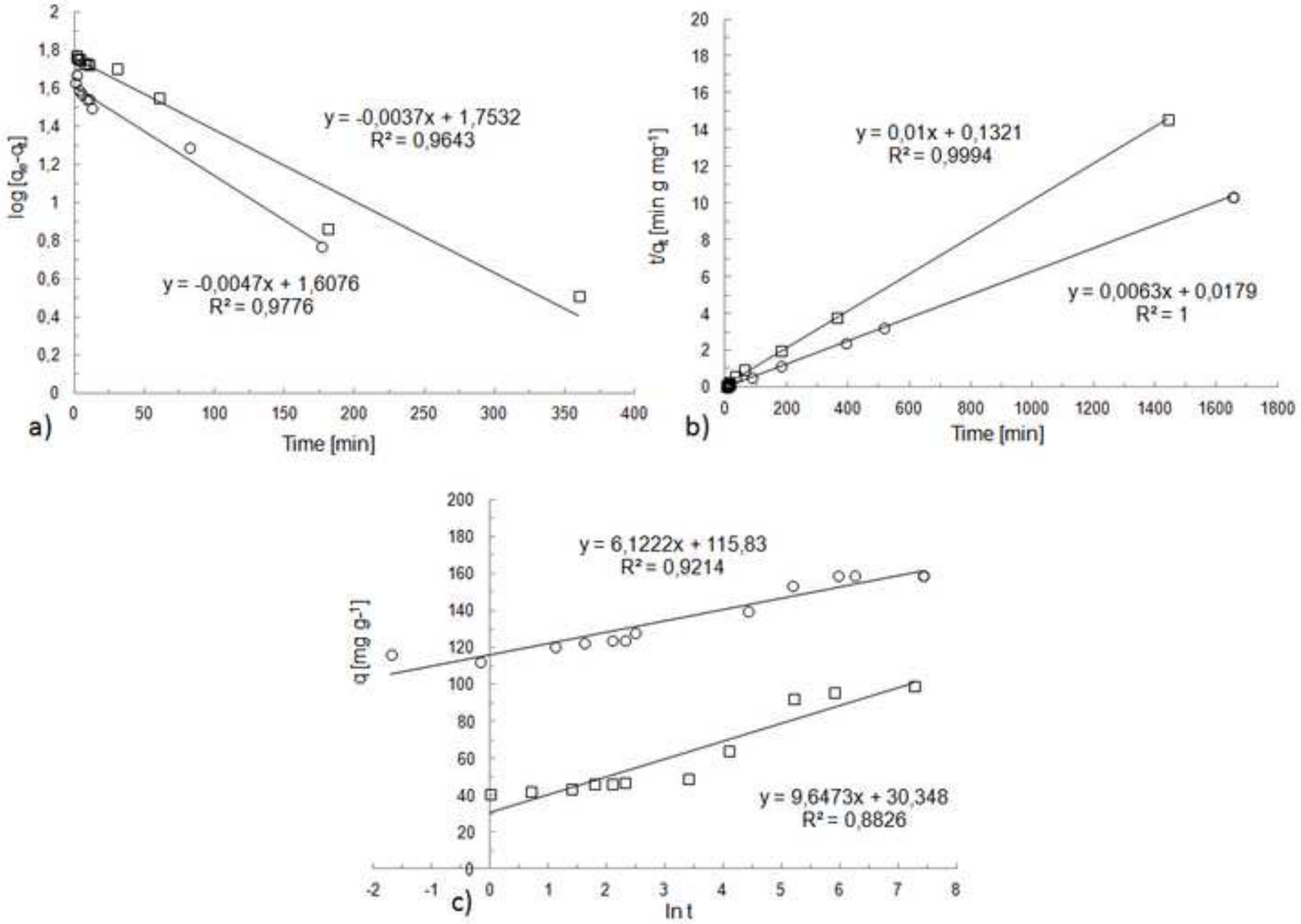

Figure 9

Click here to download high resolution image

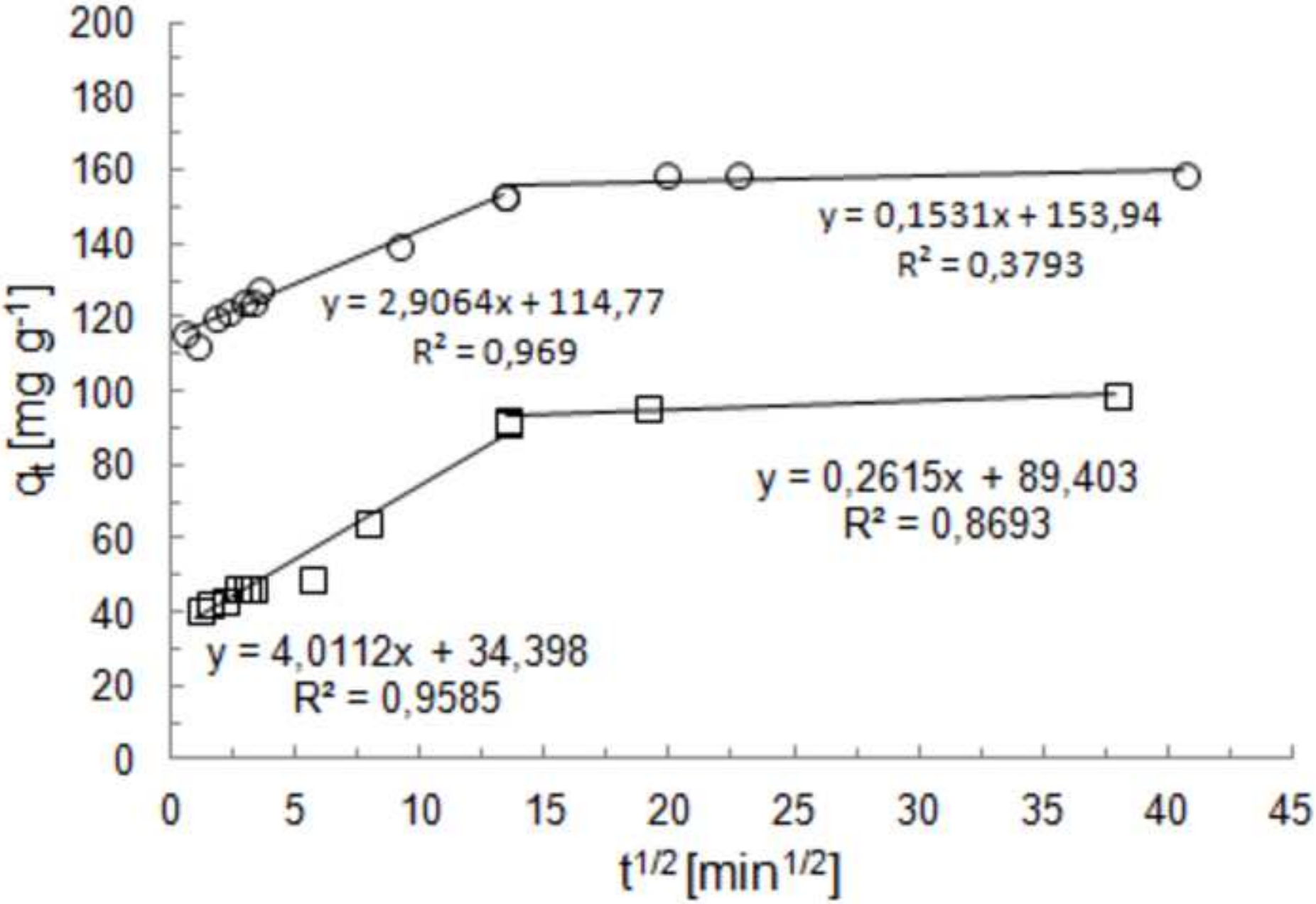

Figure 10

Click here to download high resolution image

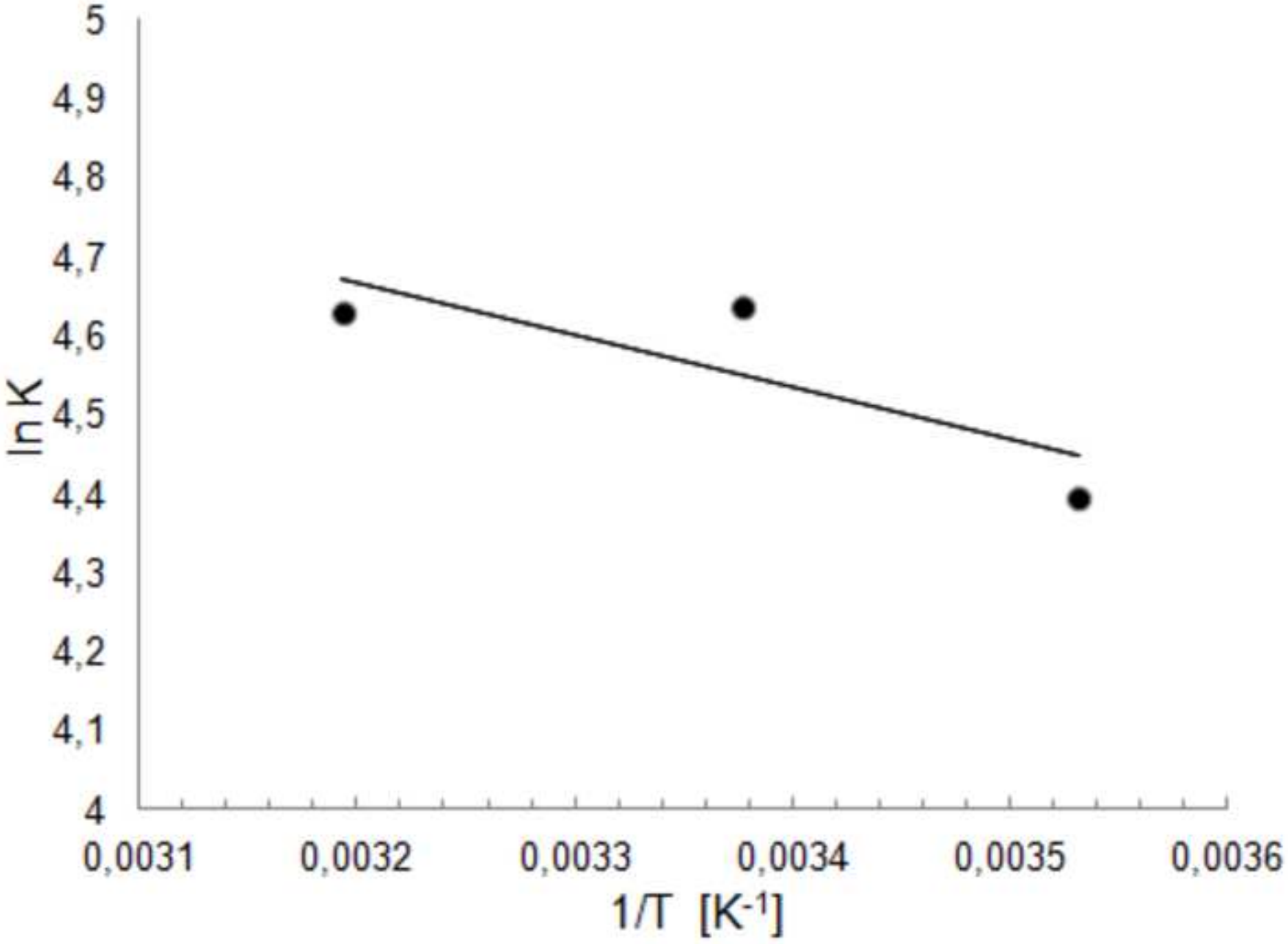

Figure 11

Click here to download high resolution image

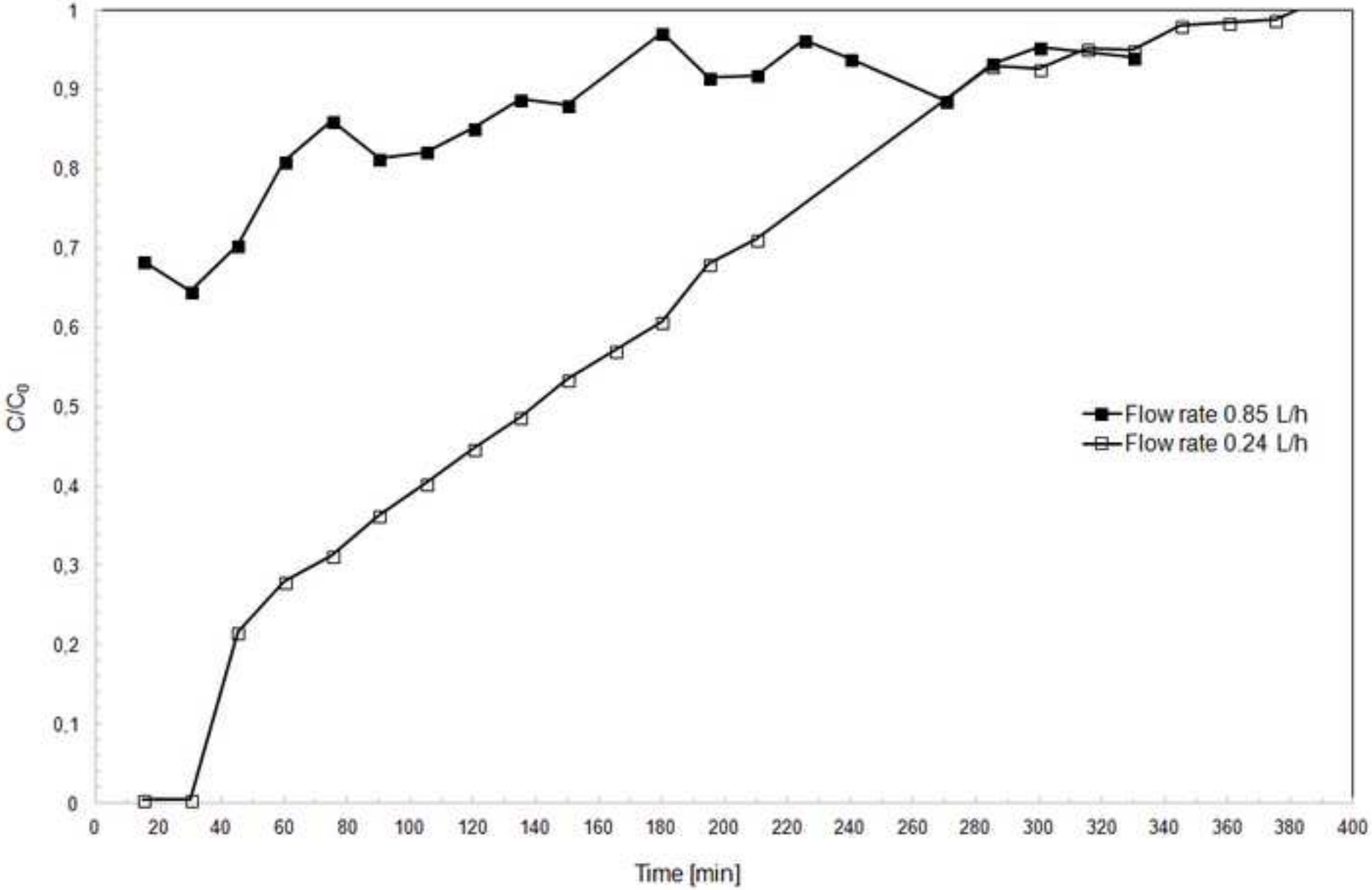

Figure captions

Click here to download Figure: Figure captions Runtti et al.docx

Figure 1. XRD patterns of blast-furnace slag (BFS), blast-furnace-slag geopolymer (BFS-GP) and barium-modified blast-furnace-slag geopolymer (Ba-BFS-GP) samples. HT = hydrotalcite, HAT = haturite, W = witherite.

Figure 2. The FTIR spectra of blast-furnace slag (BFS), barium-modified blast-furnace-slag (Ba-BFS) and barium-modified blast-furnace-slag geopolymer (Ba-BFS-GP).

Figure 3. Total SO_4^{2-} removal per cent (left, solid lines) and total adsorbed amount (right, dashed lines) versus initial pH on the sorption of SO_4^{2-} from mine effluent. Sorbent dosage: 5 g L^{-1}, contact time: 24 h, temperature: 22–23 °C, adsorbate: mine effluent (C_0, SO_4^{2-}: ~850–870 mg L^{-1}).

Figure 4. Effect of the initial concentration on the sorption of SO_4^{2-} on Ba-BFS-GP from model solution. Initial pH: 7–8, sorbent dosage: 5 g L^{-1}, contact time: 24 h, temperature: 22–23 °C.

Figure 5. Effect of Ba-BFS-GP dosage on SO_4^{2-} removal. a) Model solution: $C_0(SO_4^{2-})$: ~1200 mg L^{-1}, contact time: 3 h. b) Mine effluent: $C_0(SO_4^{2-})$: 865 mg L^{-1}, contact time: 24 h. In both cases initial pH was 7–8.

Figure 6. Bi-Langmuir, Sips, Redlich-Peterson and Toth isotherms of SO_4^{2-} sorption on Ba-BFS-GP. a) Model solution: $C_0(SO_4^{2-})$: 100–1800 mg L^{-1}, sorbent dose: 5 g L^{-1}. b) Mine effluent: $C_0(SO_4^{2-})$: 865 mg L^{-1}, sorbent dose: 1.3–15 g L^{-1}. Initial pH was 7–8, contact time 24 h and temperature 22–23 °C.

Figure 7. Effect of contact time on the removal efficiency of SO_4^{2-} onto Ba-BFS-GP. o: Model SO_4^{2-} solution (C_0, SO_4^{2-}: 1100 mg L^{-1}), □: Mine effluent (C_0, SO_4^{2-}: 853 mg L^{-1}). Initial pH: 7–8, sorbent dosage: 5 g L^{-1}, temperature: 22–23 °C.

Figure 8. a) Pseudo-first-order kinetic, b) pseudo-second-order kinetic and c) Elovich model plots of SO_4^{2-} sorption on Ba-BFS-GP. o: Model SO_4^{2-} solution (C_0, SO_4^{2-}: 1100 mg L^{-1}), □: Mine effluent (C_0, SO_4^{2-}: 853 mg L^{-1}). Initial pH: 7–8, sorbent dosage: 5 g L^{-1}, contact time: 24 h, temperature: 22–23 °C.

Figure 9. Weber and Morris intraparticle diffusion model plot of SO_4^{2-} sorption on Ba-BFS-GP. o: Model SO_4^{2-} solution (C_0, SO_4^{2-}: 1100 mg L^{-1}), □: Mine effluent (C_0, SO_4^{2-}: 853 mg L^{-1}). Initial pH: 7–8, sorbent dosage: 5 g L^{-1}, contact time: 24 h, temperature: 22–23 °C.

Figure 10. Van't Hoff plot for adsorption of SO_4^{2-} removal. Initial pH: 7–8, adsorbent dosage 5 g L^{-1}, $C_0(SO_4^{2-})$: 1200 mg L^{-1}.

Figure 11. Breakthrough curves of SO_4^{2-} by Ba-BFS-GP packed column for two different flow rates.

*Abstract

Blast-furnace slag and metakaolin were geopolymerised, modified with barium or treated with a combination of these methods in order to obtain an efficient SO_4^{2-} sorbent for mine water treatment. Of prepared materials, barium-modified blast-furnace slag geopolymer (Ba-BFS-GP) exhibited the highest SO_4^{2-} maximum sorption capacity (up to 119 mg g^{-1}) and it compared also favourably to materials reported in the literature. Therefore, Ba-BFS-GP was selected for further studies and the factors affecting to the sorption efficiency were assessed. Several isotherms were applied to describe the experimental results of Ba-BFS-GP and the Sips model showed the best fit. Kinetic studies showed that the sorption process follows the pseudo-second-order kinetics. In the dynamic removal experiments with columns, total SO_4^{2-} removal was observed initially when treating mine effluent. The novel modification method of geopolymer material proved to be technically suitable in achieving extremely low concentrations of SO_4^{2-} (< 2 mg L^{-1}) in mine effluents.